

PUNCHING-SHEAR STRENGTH OF REINFORCED CONCRETE SLABS SUBJECTED TO UNIDIRECTIONAL IN-PLANE TENSILE FORCES

Pablo G. Fernández*

Civil Engineer, MSc, PhD student
Universitat Politècnica de Catalunya
Department of Civil and Environmental Engineering
Campus Nord Jordi Girona 1-3, C-1 201, 08034 Barcelona, Spain
Phone number: +34 934015762
E-mail: pablo.gonzalo.fernandez@upc.edu

Antonio Mari

Civil Engineer, MSc, PhD
Professor
Universitat Politècnica de Catalunya
Department of Civil and Environmental Engineering
Campus Nord Jordi Girona 1-3, C-1 201, 08034 Barcelona, Spain
E-mail: antonio.mari@upc.edu

Eva Oller

Civil Engineer, MSc, PhD
Associate Professor
Universitat Politècnica de Catalunya
Department of Civil and Environmental Engineering
Campus Nord Jordi Girona 1-3, C-1 201, 08034 Barcelona, Spain
E-mail: eva.oller@upc.edu

***Corresponding author**

ABSTRACT

Some reinforced concrete slabs are subjected simultaneously to concentrated loads and unidirectional in-plane tensile forces. This the case of the top slab of a box girder bridge where hogging bending moments take place at the intermediate supports. Then, the in-plane tensile forces may reduce the punching-shear strength under concentrated loads.

This paper describes an experimental campaign carried out to investigate the effect of unidirectional in-plane tensile forces on the punching-shear strength of RC slabs. A total of 5 slabs (1650 x 1650 x 120 mm), subjected to different levels of in-plane tensile forces were tested under a concentrated load up to failure.

As observed, the punching-shear strength diminishes almost linearly as the tensile force increases, up to a certain point associated to concrete cracking. From that point on, the reduction of punching

strength is larger since the tensile force at the crack must be resisted by the reinforcement, which yields prematurely.

Keywords: Punching-shear, tension, reinforced concrete, slab, tests, punching-shear failure, concentrated load.

1. INTRODUCTION

Reinforced concrete (RC) slabs are structural elements widely used in both bridges and buildings, due to their great versatility and ease of construction. However, they have the disadvantage that the concentration of stresses in a small area, either under the wheel of a heavy vehicle or by the reaction of a column, can cause the element to fail due to punching-shear, which is a brittle and sudden failure and, therefore, undesirable from the point of view of user safety. Figure 1 shows a recent punching-shear failure of a car park in Santander (January 2020) [1].

Figure 1

RC slabs subjected to the simultaneous action of transverse concentrated loads and in-plane tensile forces can be found in continuous box girder bridges, at intermediate supports, where tensile stresses arise in top slab as result of hogging bending moments and may act together with a heavy vehicle load. Another common situation where this phenomenon takes place is on floor slabs supported on columns and subjected to a horizontal load, due to wind or earth pressure, on one of their sides. Skew compressions going from that side to the restraining columns of the opposite side may generate tensile stresses in the perpendicular direction, as can be seen in Figure 2.

Figure 2

The phenomenon of punching-shear has been extensively studied over the years, both theoretically and experimentally [2-15]. As far as the authors are aware, very few studies have been carried out regarding punching shear when there are tensile forces in the mid-plane of the slabs. Regan, in his report to the British Department of Transportation [16], presents the results of three 1.5 x 1.5 x 0.125 m slabs (BD Series) subjected to unidirectional in-plane tension and an out-of-plane concentrated load on its center, all of them with different support schema (Fig. 3-a). More recent studies have been carried out at the University of Lyon [17], regarding the influence of uniaxial tension on the shear strength of 2,6 x 4 x 0,3 m simply supported concrete slabs subjected to concentrated loads close to the support (Fig. 3-b). Both studies concluded that axial tensile stresses reduce punching and shear strength respectively, although the experimental campaigns carried out covered a limited number of in-plane tensile stress levels.

As far as most frequently used design or codes concern, such as EC-2 [18], ACI [19] or Model Code 2010 [20], each one of them contemplate the effect of in-plane normal stresses in a different way. EC-2, in section 6.4.4, includes the effect of axial stresses on punching strength by including the term $k_l \cdot \sigma_{cp}$, in (1), with $\sigma_{cp} = N_u/A_c$, being N_u the axial load applied in the cross section, but it does not differentiate between tension and compression. However, the response of the concrete in one case or in the other one is radically different.

$$V_{Rd,c} = (C_{Rd,c} \cdot k \cdot \sqrt[3]{100 \cdot \rho_l \cdot f_{ck}} + k_1 \cdot \sigma_{cp}) \cdot b_w \cdot d \quad (1)$$

ACI, in section 22.6.5 (two way shear) proposes two expressions to calculate the punching strength of a slab with an axial load due to prestressing, but no mention is made of the case of axial tension. In section 22.7.5 (one way shear), it proposes an expression for the shear strength of members subjected to “significant” axial tension (2), but what “significant” means is left to the judgement of the designer. In Eq. (2), N_u is considered negative in this equation.

$$V_c = 0.17 \cdot \left(1 + \frac{N_u}{3.5 \cdot A_c}\right) \cdot \sqrt{f_{ck}} \cdot b_w \cdot d \quad (2)$$

Finally, Model Code 2010, in section 7.3.5.3, presents an expression for the punching strength of slabs (3). This equation includes the term k_{ψ} , which depends on the load-rotation curves of the slab, whose response is different under compression or tension axial forces.

$$V_{Rd,c} = k_{\psi} \cdot \frac{\sqrt{f_{ck}}}{\gamma_c} \cdot b_0 \cdot d_v \quad (3)$$

Figure 3

In this context, an experimental campaign has been carried out at the Laboratory of Technology of Structures and Materials of the Universitat Politècnica de Catalunya (UPC), whose essential objective was to identify and quantify the effect of unidirectional in-plane tension forces on the punching-shear strength of reinforced concrete slabs. On the other hand, it is intended to provide experimental results to contribute to extend the mechanically-based punching-shear resistance model “Compression Chord Capacity Model” (CCCM) [21], developed by some of the authors, to the case of in-plane tension.

From the 5 specimens tested, one was a control slab without tensile forces (Slab A0), while the other 4 slabs were subjected to different levels of tensile force. One of the slabs (Slab B1) had a greater amount of reinforcement in the direction parallel to the tension, with the aim of studying the influence of this variable. This paper presents some results of the experimental program such as the load-displacement relationships, crack patterns at failure and strains at the reinforcement parallel to the direction of the applied tension of each test. As explained, a decrease in the ultimate load with respect to that obtained for the control slab was observed as the external tension increased. A physical interpretation of the structure behavior is made.

2. EXPERIMENTAL CAMPAIGN

2.1. Specimens tested

A total of 5 slabs of 1650 x 1650 x120 mm were cast in the lab. The dimensions of the slabs tested in the context of this experimental campaign are based on the punching-shear tests performed in [22-23]. The slabs are intended to represent a continuous building slab supported by an orthogonal column grid of 3.75 m of span length in the two orthogonal directions. The slabs were supported by 8 points placed at the vertices of a regular octagon, equidistant 765 mm from the point load vertical axis, applied on its center. Even though the specimens may be better suited to represent

deck-slab of bridges than an actual floor slab, this size was selected to give continuity to the experimental work carried out in [23], which have been a starting point for the present experimental campaign.

The slabs were subjected to tension in their plane, in only one direction, through 10 post-tensioning bars 25mm in diameter and 600mm in length, partially embedded in 2 opposite faces (5 bars on each side) (see Figs. 4 and 5). These bars were connected to the tensioning system to apply the tensile force to the slab. Although most of the tension was transmitted to the concrete by bond, anchors were placed at the embedded end of the bars for greater safety. The value of the external tension applied during the tests is measured in relation to the tensile force producing the cracking of the slab or $T_{cr} = A_c f_{ct}$, with A_c being the composite concrete and steel area of the cross-section of the slab and f_{ct} the tensile concrete strength. The specimens were designed so that punching failure takes place before flexural failure up to a value of $T = 1.5T_{cr}$, having computed the ultimate punching capacity using different formulations (EC-2 [18], EHE [24], CCCM [21]).

Figure 4

The slabs were reinforced with two steel meshes arranged on the upper and lower faces (Fig. 5). In the direction parallel to the external tension applied, the same amount of reinforcement was placed on the upper and lower faces in all the slabs (A0, A1, A2, A3, B1). This reinforcement consisted of 12mm bars spaced 105 mm in slabs type A ($\rho = 0.011$) and 16mm bars spaced 105 mm in slab B1 ($\rho = 0.0200$).

In the direction perpendicular to the applied tension, on the lower face, an assembly consisting of 12mm bars spaced 100 mm was arranged in all cases, ($\rho = 0.013$), while 12 mm bars spaced 200 mm were arranged on the upper face. Additional reinforcing bars were placed in the vicinity of the post-tensioning bar anchors, as a measure of local reinforcement. The tensile reinforcement ratio and effective depth of each type of slab are shown in Table 1.

Figure 5

The large amount of longitudinal reinforcement in specimen B ($\rho=2\%$) may give place to values of the aggregate interlock and dowel action contributions to the punching strength, higher than usual in practical cases. However, the experimental results of slab B can be adequate to identify how the increment of reinforcement ratio affects the structural response and to verify how theoretical models account for the above mentioned effects on the punching shear resisting mechanisms.

The punching load was transmitted to the slab through a 145 x 145 x 30 mm steel plate located in its center. Due to the configuration of the experiment, the slabs were tested face down with respect to their real position in a building slab, in which the reaction of the column goes upwards and the tensile reinforcement is arranged on the upper face.

The slabs were cast using ready-mixed concrete from a local supplier. Normal strength class C30/37 with crushed limestone aggregate with a maximum size of 10 mm was used. To characterize the concrete before each punching test, standard compression (UNE-EN 12390-3), splitting (UNE-EN 12390-6) and elastic modulus (UNE-EN 12390-13) tests were performed. The specimens were reinforced with deformed bars of B500-S steel. Yield stress and elastic modulus of each type of reinforcing steel (UNE-EN ISO 6892-1) were also characterized. The results are shown in Table 2.

Table 1

Table 2

2.2 Test set-up

Four out of the five tested specimens were subjected to different levels of tensile stresses, while the control slab was left un-tensioned. To introduce the tensile force in the slabs, an auxiliary steel

structure, whose plan dimensions were 2500 x 2840mm, was built. This structure consisted of a rectangular steel frame surrounding the slab (see Fig. 6).

Figure 6

On both sides parallel to the tensile forces, the frame consisted of a single HEB 300 profile, while on both perpendicular faces it was formed by two HEB 300 profiles arranged in parallel and separated four centimeters, to allow the passage of bars (extensions) connected to the above mentioned bars partially embedded in the slab. On one of these faces, a passive anchor for the tensioning bars was used whereas they were prestressed from the other end, with the help of force-controlled hollow jacks connected to the above mentioned extension bars (see Fig. 7).

Figure 7

The steel structure was set at the appropriate height with the help of four height-adjustable supports designed for the experimental campaign and located under each of the four corners of the frame. For safety reasons, once the desired external force value was reached, the bars were anchored and the jacks were disconnected from them. This fact caused a small loss of the test force during the test that was quantified by the arranged instrumentation. The theoretical loads to be applied and the values measured during the tests are shown in Table 3.

Table 3

To introduce the punching load, a hydraulic jack anchored in a loading frame, rigidly fixed to the floor slab, was used. Eight 120 x 120 mm load cells were placed at the slab supports to measure the reactions, arranged in a circle centered with respect to the center of the loading frame. A piece of rubber 120 x 120 x 20 mm was placed over each of the cells to allow free rotation in

the supports. The 8 load cells were supported on 4 rigid easels arranged in such a way that the distance between the mid-points of two opposite supports was 1530 mm. To cause the punching of the slab, a 145 x 145 x 30 mm steel loading plate was used, under which a thin layer of fine aggregate was placed to ensure regular contact between the upper face of the slab and the plate (see Fig. 8).

Figure 8

Due to the small distance between the bars protruding from the slabs and the steel frame, the evolution of the reaction force yielded by the nearest load cells to the frame was closely monitored in order to observe a possible interaction between both elements. Only in the test with the highest tensile force, and also the highest deflection, a slower increment of those reactions was observed close to the end of the loading stage, which may indicate some contact between the protruding bars and the frame. This interaction resulted in a slight decrement of these reaction forces, about a 5% of the mean reaction at each support, at the failure load. Therefore, this effect has been neglected.

2.3 Instrumentation

Load cells of 50 kN were used as supports of the slab in the position given in Figure 8. In addition, hollow load cells of 500 kN were used in the post-tensioned bars, (in both active and passive anchors), in order to measure the in-plane tensile force applied to the slab. To control the deformation and the entry of the reinforcement into plastic regime, 32 strain gauges were distributed throughout the slab, 24 of which were placed in the reinforcement parallel to the tension and 8 in the perpendicular reinforcement, also in the central section (see Fig. 9). In addition, a 75 mm displacement transducer was placed in the center of the lower face to measure the vertical displacement at the center of the slab, jointly with the internal linear variable displacement transducer (LVDT) of the loading frame. Finally, 8 LVDTs on the upper side of the slab were located, in the vertical of each support, to control their descent and subtract their mean value from the displacements measured in the center of the slab.

Figure 9

2.4. Test procedure

First, the tensile force, given in Table 3, was introduced in the slabs and, subsequently, the point load was incrementally applied on its center up to failure of the slab. In all cases, two levels of the vertical load were previously applied, one up to 20% of the predicted ultimate load (P_u) and another up to 40% of P_u . Both loads were maintained for 100 seconds and served to accommodate all the elements involved in the test and to check that the instrumentation was properly working. Once the second test load ended and the slab was unloaded, the test up to failure was started, applying the load by a controlled displacement at a rate of 0.001mm/s. Taking account of the stretching of bars and the loading stages, average test duration was about two and a half hours.

In support of the experimental campaign, a finite element model was developed, using as reference the one developed at the University of Waterloo (Canada) by Polak et al [22]. This model was initially used to predict the tests results and to design the auxiliary structures of loading and support.

Once the first test was performed over the reference slab A0, the numerical model was calibrated with the obtained results, see Figure 10, and used to predict the results of the rest of Type-A slabs, under different tensile force levels. With respect to the Type B slab, only a test was performed with a tensile force of $T/T_{cr}=0.5$. Then, since there was not reference slab of type B, the same numerical model was also used to predict the punching capacity of the Type B reference slab, as shown in Table 4. Details of the numerical simulations performed will be explained in Section 4.

Figure 10

Table 4

3. EXPERIMENTAL RESULTS

3.1. Ultimate loads

The main interest of the experimental campaign was to observe the variation of the ultimate punching-shear load as a function of the tension force applied to the slabs. For this purpose, the load-displacement curves of each of the tests are analyzed in this section, together with that obtained for the control slab. Table 5 shows the punching-shear failure load of each test and also their relationship with that of the control slab (see also Figure 11).

Figure 11

As can be seen, there is a notable and progressive reduction in the failure load with respect to the value obtained in the control slabs. The maximum reduction was 28% for $T = 1.26 T_{cr}$. The decreasing trend is practically linear with the applied tensile force and is accentuated in cases where the applied tensile force is greater or equal than T_{cr} . This is possibly due to the fact that when the value of T_{cr} is exceeded, cracking of the concrete occurs and, at the crack, the entire value of the applied external tension is resisted by the reinforcement, which increases dramatically its stress, reducing its contribution to the punching strength. Figure 12 shows the load vs. displacement at the center of slab for all type-A specimens. The previous explanation can also be applied to the increase in the ultimate displacement as long as the tensile force increases. The premature yielding of the reinforcement decreases the stiffness of the piece and, therefore, an increase in the deflection occurs.

Table 5

Figure 13

Figure 13 shows the state of cracking at the bottom face of the slab at failure for some of the tests carried out (tensile forces are in the vertical direction). As observed, the crack pattern area increases in the dimension perpendicular to the tensile forces, as the applied tensile force increases.

3.2 Strains at the reinforcement

In order to know the state of the reinforcement at failure, the strain was measured in gauges glued in the central area of the slab, in rebars parallel to the tensile force (gauges from 3 to 6) and perpendicular to it (gauges from 11 to 14). For the reinforcement parallel to the applied tensile force, it was observed that, while in the control slab yielding of the reinforcements occurred for a load close to the punching-shear failure load, in the tensioned specimens such yielding occurred clearly before failure (see Fig. 14).

In Figure 14, it can also be seen how the rate of strain measured in the gauges located in the reinforcement perpendicular to the tension increases slightly after the gauges of the parallel reinforcement enter in the plastic regime. This indicates that there was a redistribution process between the reinforcement of both directions. The evolution of the average strain of the reinforcement located in the central zone in both directions is shown in Figure 15.

Figure 13

Figure 14

Figure 15

4. NUMERICAL SIMULATIONS

In addition to help in the design of the tests setup, the numerical model is being used to contrast the values of the punching strength obtained by the Compression Chord Capacity Model, CCCM, [21] extended to punching with tension, both for the tests performed and for values of tension forces different from those applied in the experimental campaign. The simulations of the experimental campaign were carried out with Simulia Abaqus software [25].

4.1 Model generation

Taking into account the existing double symmetry, both in geometry and loading, only a quarter of each slab was simulated, considering the corresponding boundary conditions in both symmetry planes. Given the similarity of the dimensions of the specimens tested with those of [23], the recommendations of [22] regarding the size of the element and the type of element used for concrete and reinforcement have been followed. For concrete, cubic elements of 8 nodes (C3D8R) have been used to reduce the computational cost and to avoid obtaining excessively rigid results [25], while for the reinforcing bars, linear beam elements of 2 nodes (B31) have been used. The reinforcing bars were considered perfectly bonded to the concrete. The size chosen for the concrete elements was 20 mm, so that 6 elements were arranged along the 120 mm of the slab edge. The supports of the slab were simulated by means of non-linear springs (SPRING A), with a very high stiffness in compression and practically zero stiffness in tension, thus allowing the partial lifting of the slab and avoiding the appearance of undesired tensile reactions (Fig. 16) The introduction of tensile forces was simulated in the model by applying the loads directly to the nodes located in the area of the anchor plates of the post-tensioning bars, while for the punching load, a displacement was imposed on the nodes located on the upper face of the slab, under the surface occupied by the load plate.

Figure 16

Abaqus offers two different packages to perform this type of simulations: Abaqus / Standard, for static analysis; and Abaqus / Explicit, for quasi-static analysis. Up to a certain value of the applied external tension ($T/T_{cr} \leq 0.8$), the results obtained with one or another form of analysis were quite similar (Fig. 17). The main difference was the time needed to perform the simulation, being more than 3 hours in the case of Abaqus / Standard and approximately half an hour in the case of Abaqus / Explicit. From $T/T_{cr} = 1$, simulations with Abaqus / Standard began to show convergence problems, so it was decided to conduct the study with Abaqus / Explicit.

Figure 17

4.2 Materials

To simulate the behavior of concrete, the Concrete Damaged Plasticity model [26], [27] was chosen, which requires the definition of the uniaxial constitutive equations in compression and tension, in addition to the definition of a yielding surface. For compression, a linear behavior of up to 40% of f_c (σ_{c0}) was considered. To define the elastic response, only the modulus of elasticity (E_c) and the Poisson ratio (ν) are needed. The modulus of elasticity is that obtained in the corresponding characterization test (see Table 2), while for ν , as Abaqus considers it a fixed value throughout the whole simulation process, including the post-cracking regime, a value $\nu = 0$ was chosen.

To take into account the non-linear behavior in compression, the Hognestad parabolic constitutive equation was chosen (see Figure 18-a). The values of ε_{c0} and ε_{cu} correspond to those proposed in Table 3.1 obtained from EC-2 [18], with values of $\varepsilon_{c0} = 0.002$ and $\varepsilon_{cu} = 0.0035$. For the tensile behavior, the model proposed in section 5.1.8.2 of the Model Code 2010 [20] has been used, which considers a linear behavior up to f_{ct} , and a bilinear softening branch governed by the fracture energy of the material (Figure 18-b). The value of the fracture energy adopted is given equation (4), proposed in [28] as a modification of that provided by the Model Code 2010 [20] to account for the maximum aggregate size of concrete, which in this case was 10 mm.

$$G_f = 0.028 f_c^{0.28} d_{dmax}^{0.32} \quad (4)$$

Figure 18

The behavior of concrete in tension must be introduced in ABAQUS through a stress-strain relationship, so it is necessary to transform the stress-crack opening given by Model Code (Figure 16) into a stress-strain curve. For this purpose, the crack opening is divided by the characteristic length of the element (l_c), defined as the average dimension of a finite element, in this case the length of an edge of a cubic element. Thus, the softening of the tensile branch, is given by $\varepsilon_{ct} = \varepsilon_{cr} + w / l_c$, where ε_{cr} is the concrete strain corresponding to the tensile strength, f_{ct} .

The values used to define the yielding surface were modified from those proposed in [20] to adjust the simulation of the type-A control slab to the results obtained in the laboratory, and are collected in Table 6. For the steel reinforcement, a uniaxial bilinear stress-strain diagram was used, considering perfect plasticity. The yield stress and the modulus of elasticity used were those extracted from the characterization tests and collected in Table 2.

Table 6

4.3 Results

A comparison between the load-displacement curves obtained by the numerical simulations and those obtained in the tests is shown in Figure 19. As can be seen in Table 7, quite accurate results were obtained in terms of the ultimate load.

Figure 19

Once it was verified that the numerical model correctly reproduced the results obtained in the laboratory tests, simulations with reinforcement ratios corresponding to type A slabs, were

performed for other T/T_{cr} values, up to a maximum of $T/T_{cr} = 1.5$. Figure 18 shows the numerically obtained punching strength decrease as T/T_{cr} increases, where the experimental results are also included. As can be seen in Figure 20, the relative decrease of strength obtained for type B slab ($T/T_{cr} = 0.44$) fits the obtained curve quite well. Thus, no favorable effect of having a greater amount of reinforcement in the direction parallel to the tensile force has been observed, except a higher value of T_{cr} .

Table 7

Figure 20

Finally, cracking patterns obtained for different values of applied external tension are presented in Fig. 21, where the variation thereof can be seen as the external tension is increased.

Figure 21

5. Conclusions

Based on the observations made during the experimental campaign and the results presented in this article, the following conclusions can be drawn:

1. Punching-shear strength of reinforced concrete slabs is reduced by the presence of an in-plane tensile force.
2. The decrease in the punching-shear strength can be well characterized by a bilinear function of the applied tensile force “ T ”. The first branch arrives up to a certain value “ T_{cr} ”, after which a higher reduction of the punching strength is observed.

3. The force " T_{cr} " is associated to that producing cracking of concrete under pure tension, after which the tensile force in the crack is fully resisted by the reinforcement parallel to the tensile force, which considerably increases its stress. Such increment of stress produces premature yielding, followed by a redistribution of stresses between the reinforcements parallel and perpendicular to the tensile force direction. Consequently, a higher reduction of the punching strength than for slabs with $T < T_{cr}$ is observed.
4. The maximum value of the reduction produced by the presence of a tensile force, for the tests carried out, was 28% with respect to the reference slab, for a load $T = 1.26 T_{cr}$. For the tensile value $T = T_{cr}$, the punching load reduction was approximately 20%
5. No favorable effect of having a greater amount of reinforcement in the direction parallel to the tension has been observed.
6. The numerical model developed, for the non-linear analysis of the tested slabs, using program ABAQUS with solid finite element analysis, once calibrated with the experimental results of the tested reference slab ($T=0$), has been a very useful tool to predict the tests results of the tests with applied in plane tensile forces and analyze possible local effects during the stressing operation.
7. The reduction of the punching strength due to the effect of the in-plane tensile force introduced, as well as its effects on the crack patterns and on reinforcement yielding have been very well predicted by the numerical model.

Acknowledgements

This work has been carried out within the framework of the research project BIA-2015-64672-C4-1-R, financed by the Ministry of Economy and Competitiveness (MINECO) of Spain, and with the invaluable help of the technicians and the director of the Structural Technology Laboratory of the Polytechnic University of Catalonia. The authors want also to thank Master students Magí Domingo and Laura Beltran who collaborated in the numerical predictions and execution of the tests, respectively.

References

- [1] Roman G. Aguilera (EFE) “Se hunde un parque infantil sobre un parking en Santander” <https://www.lavanguardia.com/sucesos/20200113/472858427145/hunde-parque-infantil-santander.html>: 2020.
- [2] Kinnunen S, Nylander H. Punching of concrete slabs without shear reinforcement. Transactions No. 158; Royal Institute of Technology; Stockholm: 1960
- [3] Moe J. Shearing strength of reinforced concrete slabs and footings under concentrated loads. Portland Cement Association, Research and Development Laboratories, vol. D47, Illinois: 1961.
- [4] Braestrup MW, Nielson MP, Jensen BC, Bach F. Axissymmetric punching of plain and reinforced concrete vol. 75. Structure Research Laboratory, Technical University of Denmark; 1976
- [5] Bazant ZP, Cao Z. Size effect in punching shear failure of slabs. ACI Struct J 1987; 84: 44-53. <http://dx.doi.org/10.14359/2785>.
- [6] Broms CE. Punching of flat plates. A question of concrete properties in biaxial compression and size effect. ACI Struct J 1990;87:292-204. <http://dx.doi.org/10.14359/2624>.
- [7] Shehata IAEM. Simplified model for estimating the punching resistance of reinforced concrete slabs. Master Struct 1990;23:364-71. <http://dx.doi.org/10.1007/BF02472716>
- [8] Bortolotti L. Punching shear strength in concrete slabs. ACI Struct J 1991;87:208-19. <http://dx.doi.org/10.14359/2717>.
- [9] Menétrey P. Analytical model for punching strength prediction. Int Work Punching Shear Capacity RC Slabs, Stockholm: 2000. p. 190-9.
- [10] Muttoni A. Punching shear strength of reinforced concrete slabs without transverse reinforcement. ACI Struct J 2008;105:440-50
- [11] Guandalini S, Burdet OL, Muttoni A.. Punching test of slabs with low reinforcement ratios. ACI Struct J 2009;106:87-95 <http://dx.doi.org/10.14359/56287>
- [12] Ospina CE, Birkle G, Widiyanto. Databank of concentric punching shear tests of two way concentric slabs without shear reinforcement at interior supports. Struct Congr 2012,

- Reston, VA: American Society of Civil Engineers; 2012. P 1814-32.
<http://dx.doi.org/10.1061/9780784412367.160>.
- [13] Fédération International du Béton (fib). Punching of structural concrete slabs. Bulletin 12. Lausanne: International Federation for Structural Concrete; 2001.
- [14] Polak MA. SP-232: Punching shear in reinforced concrete slabs. Am Concrete Institute, Spec Publ, vol. 232; 2005. P.302. <http://dx.doi.org/10.14359/14960>.
- [15] Koppitz R, Kenel A, Keller T. Punching shear of RC flat slabs – Review of analytical models for new and strengthening of existing slabs. Eng Struct 2013;52:123-30.
<http://dx.doi.org/10.1016/J.ENGSTRUCT.2013.02.014>.
- [16] Regan, PE. Punching shear in prestressed concrete slab bridges. Engineering Structures Research Group, Polytechnic of Central London, 1983.
- [17] Bui TT, Nana WSA, Abouri S, Liman A, Tedoldi B, Roure T. Influence of uniaxial tension and compression on shear strength of concrete slabs without shear reinforcement under concentrated loads. Construction and Building Materials 2017;147:86-101
- [18] European Committee for Standardization. Eurocode 2: design of concrete structures: Part 1: general rules and rules for buildings. Brussels, Belgium: European Committee for Standardization; 2002
- [19] ACI (American Concrete Institute). Building code requirements for structural concrete and commentary. ACI 318 2014;Farmington:519
- [20] Fédération internationale du Béton. Fib Model Code for Concrete Structures 2010 xol. 1. Lausanne: Ernst & Sohn; 2013
- [21] Marí A, Cladera A, Oller E, Bairán JM. A punching shear mechanical model for reinforced concrete flat slabs with and without shear reinforcement. Engineering Structures 2018;166:413-26
- [22] Genikomsou A, Polak MA. A Finite Element analysis of punching shear of concrete slabs using damaged plasticity model in ABAQUS. Eng. Structures 2015;98:38-48
- [23] Adetifa B, Polak MA. Retrofit of slab column interior connections using shear using shear bolts. ACI Struct J 2005;102:268-74. <http://dx.doi.org/10.14359/14278>.

- [24] Comisión Permanente del Hormigón. Instrucción de Hormigón estructural EHE-08. Madrid, España: Ministerio de Fomento; 2011
- [25] Abaqus Analysis user's manual 6.14, Dassault Systems Simulia Corp., Providence, RI, USA; 2014
- [26] Lubliner J, Oliver J, Oller S, Oñate E. A plastic-damage model for concrete. *Int J Solids Struct* 1988;25(3):299-326
- [27] Lee J, Fenves GL. Plastic-damage model for cyclic loading of concrete structures. *J Eng Mech* 1998;124(8)892-900
- [28] Cladera, A., Marí, A., Bairán, JM. Oller, E., Duarte, N. (2016) "The compression chord capacity model for the shear design and assessment of reinforced and prestressed concrete beams" *Structural Concrete (fib)*, Wiley, 18-2, pp1017-1032, ISSN 1464-4177

List of Figures

Figure 1. Collapse of an underground car park due to Punching in Santander, Spain (2020) [1].

Figure 2. Common situations where in-plane tensile stresses and a concentrated load may act together

Figure 3. Schema of the tests carried out by a) Regan b) at the University of Lyon

Figure 4. Position of post tensioning bars inside the reinforcement

Figure 5. Reinforcement layout of “type A” slabs. a) Tension side. b) Compression side.

Figure 6. Steel frame used to apply tensile force to the slabs.

Figure 7. a) Jacks placed at the active anchorage. b) Passive anchorage.

Figure 8. a) Support scheme. b) Hydraulic jack used to apply the punching load. c) Fine aggregate layer.

Figure 9. Position of strain gauges on the reinforcement.

Figure 10. Load-deflection curve of the “A” control slab obtained in the lab test and with FEA.

Figure 11. Relative decrement of the punching strength to the tensile force applied.

Figure 12. Load-deflection curves of the 4 “A” specimens.

Figure 13. Final crack pattern of the slabs: a) $T=0$; b) $T=0.69T_{cr}$; c) $T=1.26T_{cr}$ (Top face); d) $T=1.26T_{cr}$. Tensile force applied in vertical direction in the photographs.

Figure 14. Evolution of strains in the reinforcement parallel to the tensile force: a) $T=0$; b) $T=0.69T_{cr}$; c) $T=1.02T_{cr}$.

Figure 15. Relation between strains in the reinforcement parallel and perpendicular to the tensile force. a) $T=0$; b) $T=0.69T_{cr}$; c) $T=1.02T_{cr}$.

Figure 16. Modelling techniques: a) Springs simulating the supports; b) cracks (in blue) in the slab after applying the tensile force (in vertical direction in the picture) at the selected nodes.

Figure 17. Comparison between load-deflection curves obtained with Abaqus/Standard and Abaqus/Explicit for $T=0$ and $T/T_{cr}=0.8$

Figure 18. a) Uniaxial compressive stress-strain relationship for concrete. b) Uniaxial tensile stress-crack width relationship for concrete

Figure 19. Comparison between load-deflection curves obtained with the numerical model and in the laboratory tests for a) $T=0$; b) $T/T_{cr}=0.44$; c) $T/T_{cr}=0.69$; d) $T/T_{cr}=1.02$; e) $T/T_{cr}=1.26$.

Figure 20. Comparison of the relative decrement of the punching strength to the tensile force applied obtained numerically and in laboratory tests.

Figure 21. Cracking pattern at failure for a) $T=0$; b) $T/T_{cr}=0.7$; c) $T/T_{cr}=1.26$; (Tensile force applied in vertical direction)

List of Tables

Table 1. Reinforcement ratios and effective depths of the tension side reinforcement.

Table 2. Mean values of material properties

Table 3. Values of the tensile force applied at each test

Table 4. Punching strength values of both types of control slabs

Table 5. Test results.

Table 6. Parameters defined for the Concrete Damaged Plasticity.

Table 7. Comparison between numerical and experimental results.

Table 1. Reinforcement ratios and effective depths of the tension side reinforcement.

Slab type	Parallel to tension			Perpendicular to tension		
	Reinforcement area (mm ²)	Reinforcement ratio	Effective depth (mm)	Reinforcement area (mm ²)	Reinforcement ratio	Effective depth (mm)
A	1810	0.0108	99	1810	0.0130	87
B	3217	0.0197	97	1810	0.0133	85

Table 2. Mean values of material properties

Concrete					
T/T _{cr}	f _c (Mpa)	f _{ct} (Mpa)	E _c (Gpa)	d_max (mm)	Age (days)
0	37.6	3.38	29.2	10	160
0.44	37.7	3.41	29.8	10	225
0.69	35.9	3.05	28.3	10	204
1.02	37.4	3.13	29.0	10	183
1.26	36.7	3.36	30.3	10	218

Steel		
Diameter (mm)	f _y (MPa)	E _s (MPa)
10	525.9	216.3
12	535.9	210.7
16	536.8	201.6

Table 3. Values of the tensile force applied at each test

Test #	Type of slab	T/T _{cr} before disconnecting jacks	T/T _{cr} at the test beginning	T/T _{cr} at failure
1	A	0.00	0.00	0.00
2	B	0.50	0.46	0.44
3	A	0.80	0.71	0.69
4	A	1.10	1.09	1.02
5	A	1.40	1.37	1.26

Table 4. Punching strength values of both types of control slabs

Type of slab	Punching shear strength (kN)	Type of analysis
A	249.1	Lab. Test
B	263.9	FEM

Table 5. Test results.

Test N°	Slab type	T/T _{cr} at failure	Punching load (P _u) (kN)	P _u /P _{control}
1	A	0	249.13	1
2	B	0.44	240.4	0.911
3	A	0.69	215.2	0.864
4	A	1.02	198.4	0.796
5	A	1.26	179.4	0.720

Table 6. Parameters defined for the Concrete Damaged Plasticity.

Dilation (ψ)	Eccentricity (ε)	σ_{b0}/σ_{co}	K	Viscosity (μ)
37.5	0.1	1.16	0.8	0

Table 7. Comparison between numerical and experimental results.

Test N°	T/T _{cr}	P _u (Numerical) (kN)	P _u (Experimental) (kN)	P _u /P _{control} (Numerical)	P _u /P _{control} (Exp.)	Δ (%)
1	0	250.3	249.13	1	1	-----
2	0.44	243.3	240.4	0.922	0.911	+1.21
3	0.69	220.3	215.2	0.880	0.864	+1.85
4	1.02	203.5	198.4	0.785	0.796	-1.38
5	1.26	182.2	179.4	0.723	0.720	+0.42



Fig. 1. Collapse of an underground car park due to Punching in Santander, Spain (2020) [1].

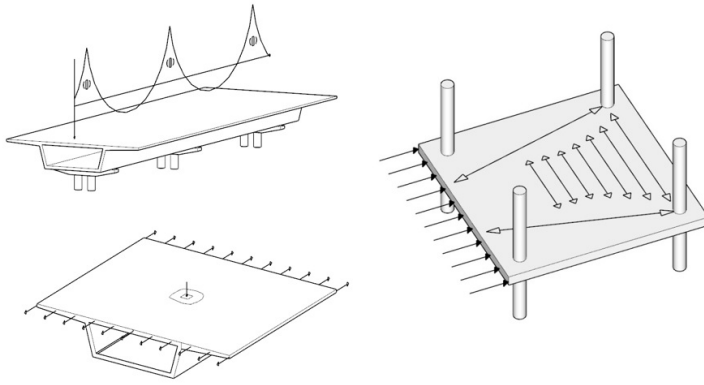


Fig. 2. Common situations where in-plane tensile stresses and a concentrated load may act together

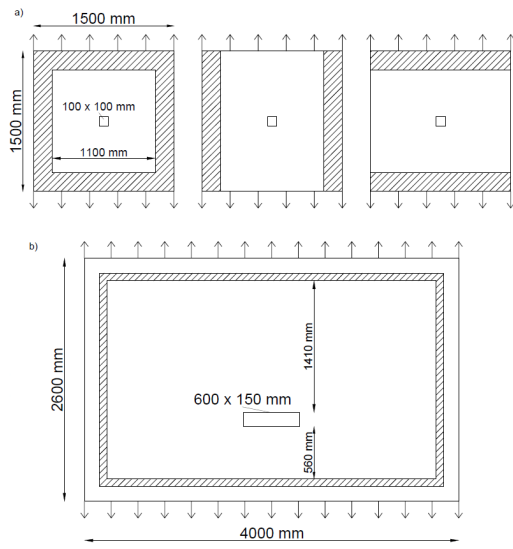


Fig. 3. Schema of the tests carried out by a) Regan b) at the University of Lyon

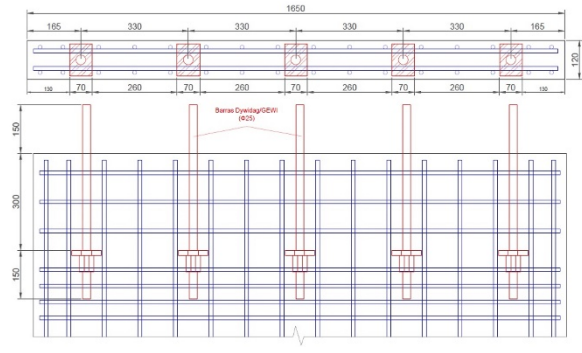


Fig. 4. Position of post tensioning bars inside the reinforcement

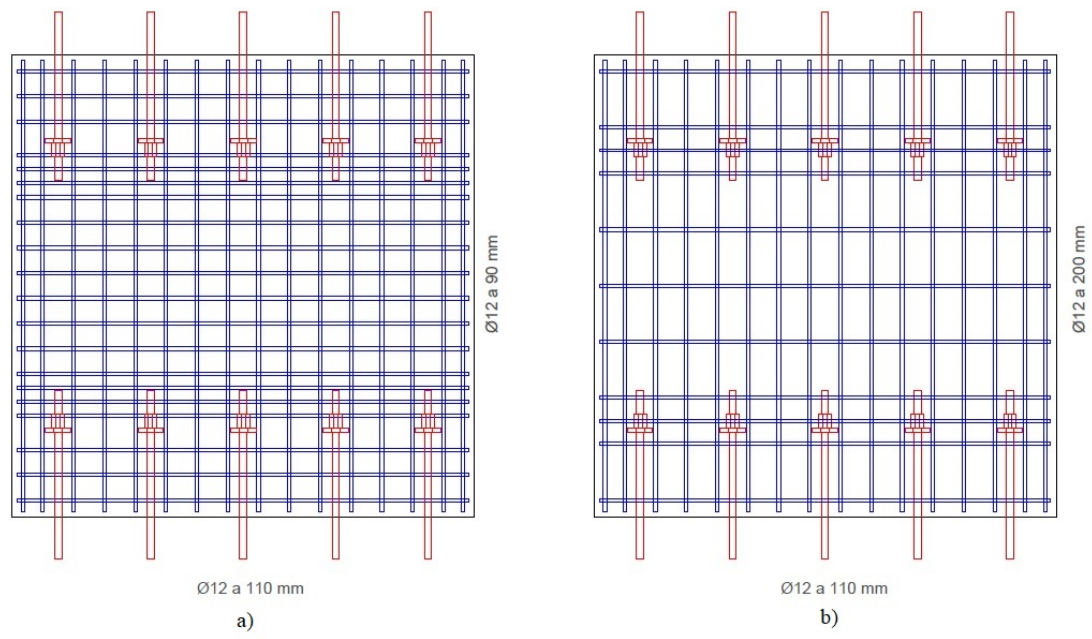


Fig. 5. Reinforcement layout of “type A” slabs. a) Tension side. b) Compression side.

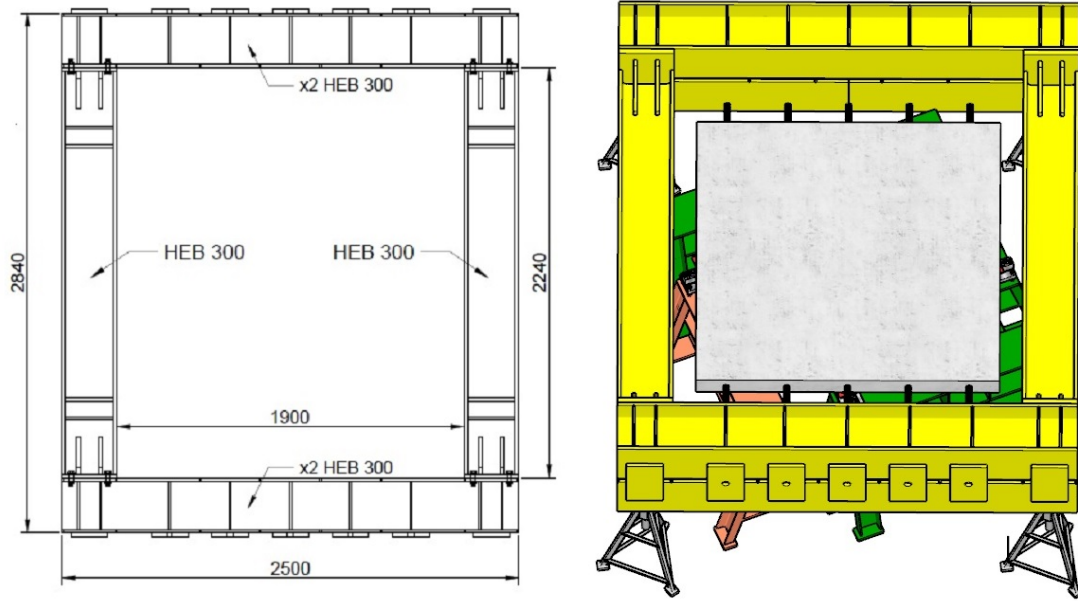


Fig. 6. Steel frame used to apply tensile force to the slabs.



a)

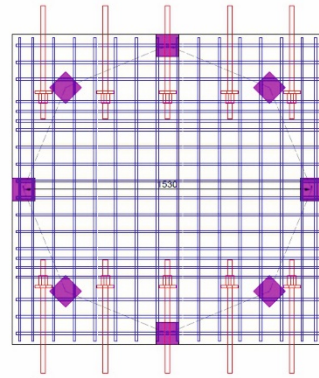


b)

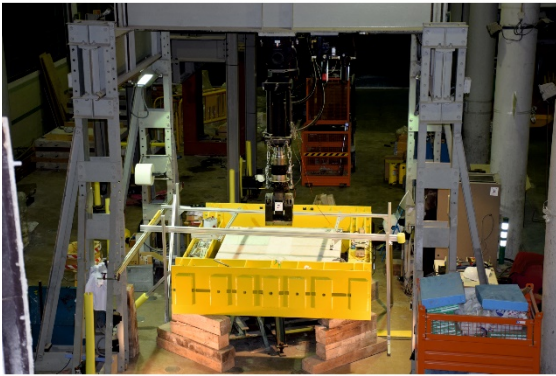
Fig. 7. a) Jacks placed at the active anchorage. b) Passive anchorage.



a-1)



a-2)



b)



c)

Fig. 8. a) Support scheme. b) Hydraulic jack used to apply the punching load. c) Fine aggregate layer.

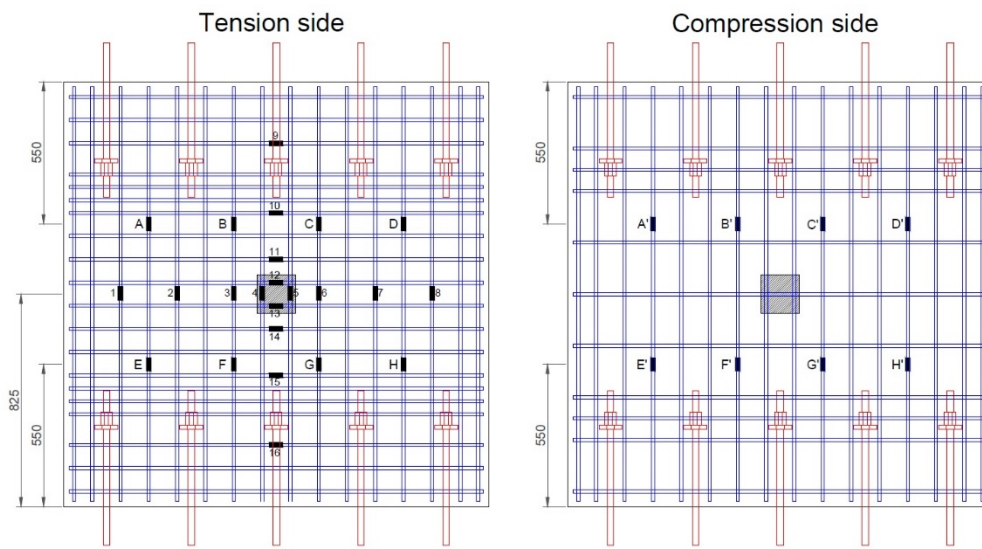


Fig. 9. Position of strain gauges on the reinforcement.

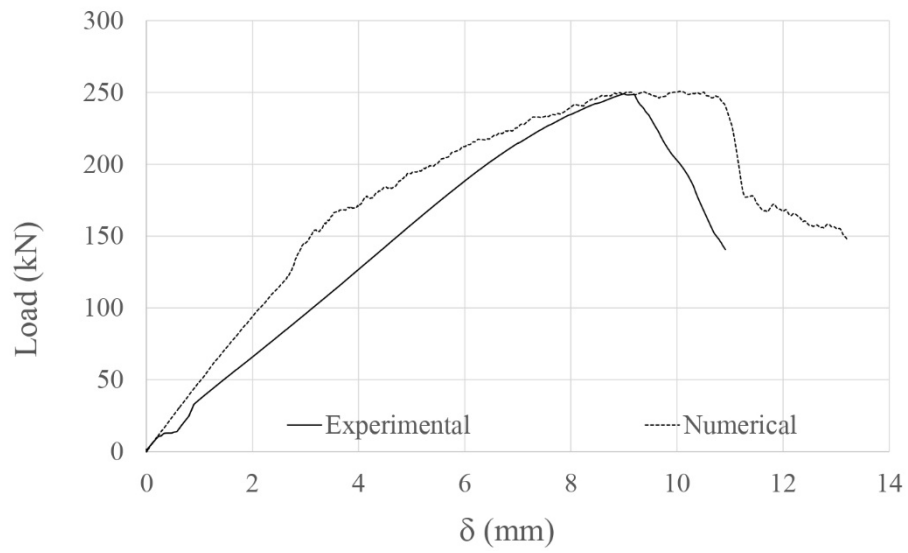


Fig. 10. Load-deflection curve of the “A” control slab obtained in the lab test and with FEA.

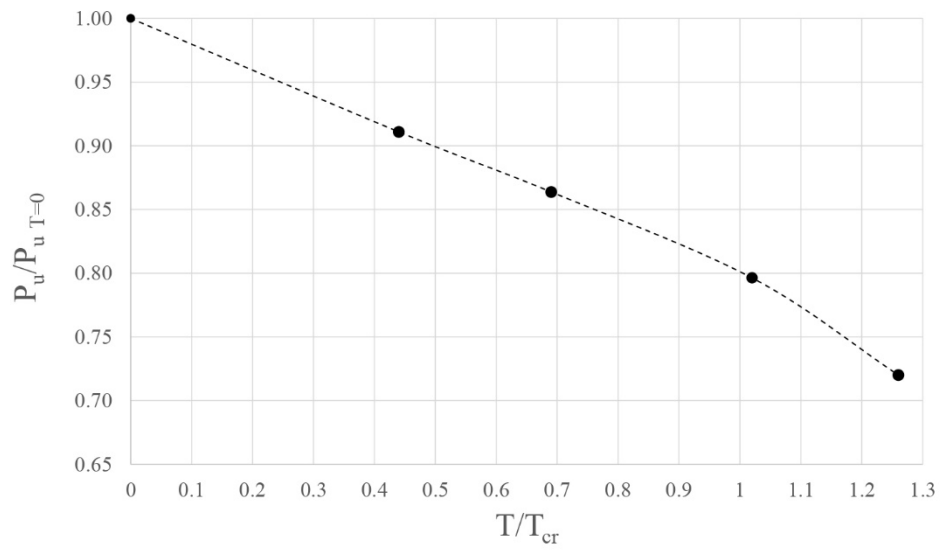


Fig. 11. Relative decrement of the punching strength to the tensile force applied.

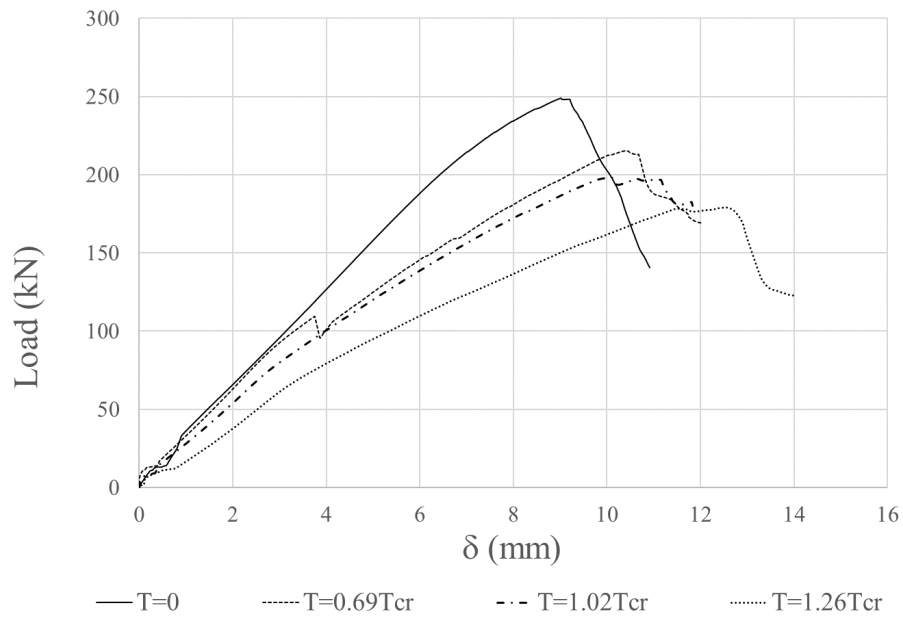


Fig. 12. Load-deflection curves of the 4 “A” specimens.

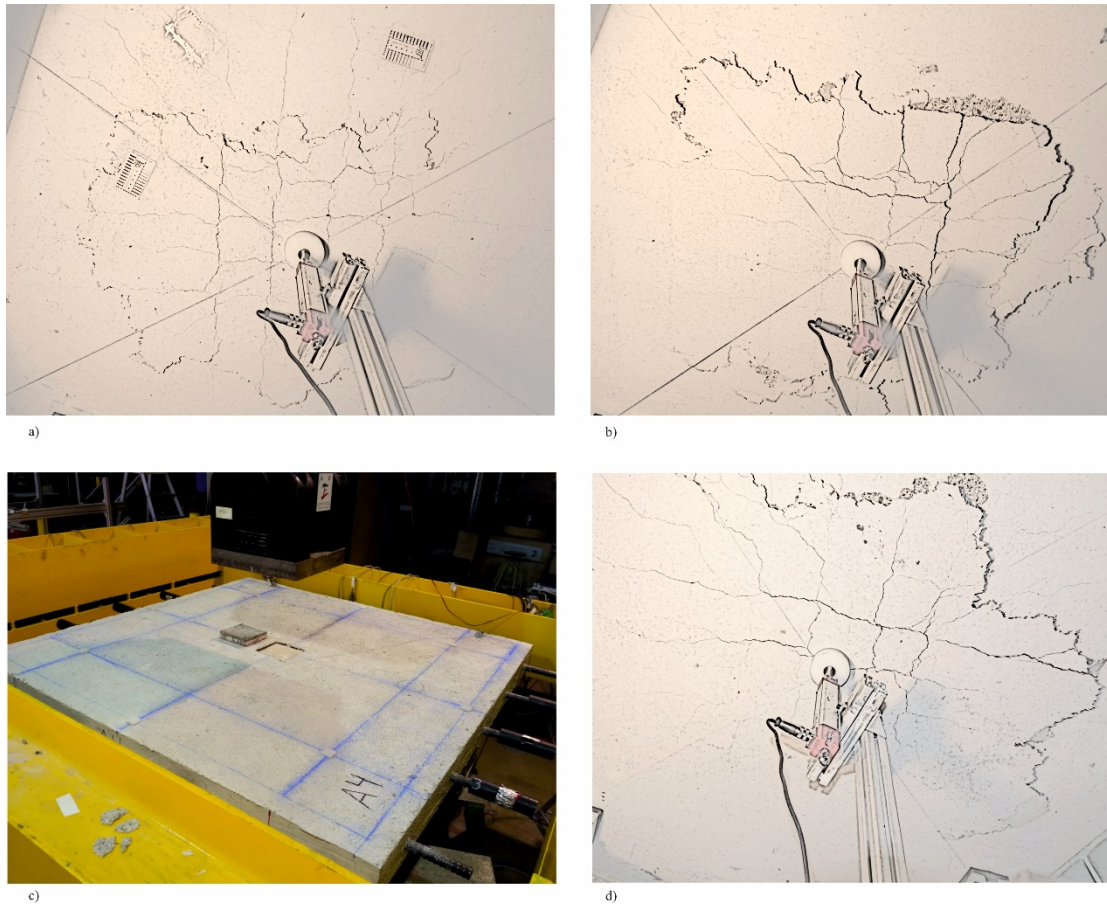


Fig. 13. Final crack pattern of the slabs: a) $T=0$; b) $T=0.69T_{cr}$; c) $T=1.26T_{cr}$ (Top face); d) $T=1.26T_{cr}$. Tensile force applied in vertical direction in the photographs.

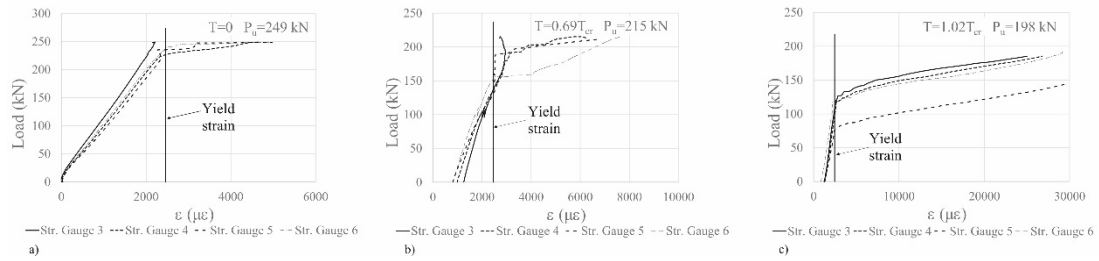


Fig. 14. Evolution of strains in the reinforcement parallel to the tensile force: a) $T=0$; b) $T=0.69T_{cr}$; c) $T=1.02T_{cr}$.

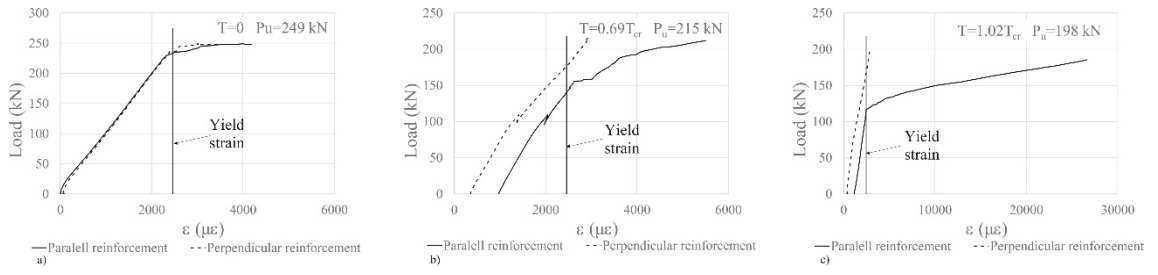


Fig. 15. Relation between strains in the reinforcement parallel and perpendicular to the tensile force. a) $T=0$; b)

$T=0.69T_{cr}$; c) $T=1.02T_{cr}$.

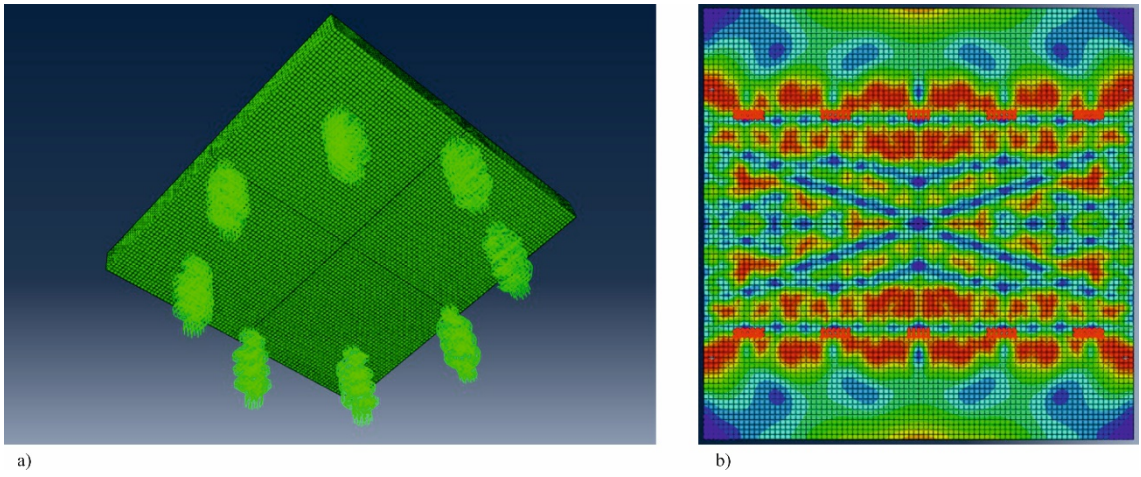


Fig. 16. Modelling techniques: a) Springs simulating the supports ; b) cracks (in blue) in the slab after applying the tensile force (in vertical direction in the picture) at the selected nodes.

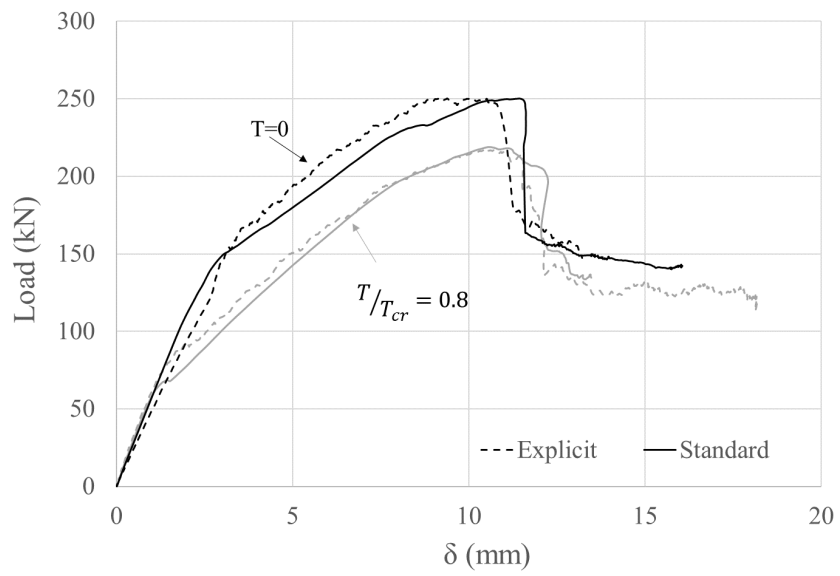
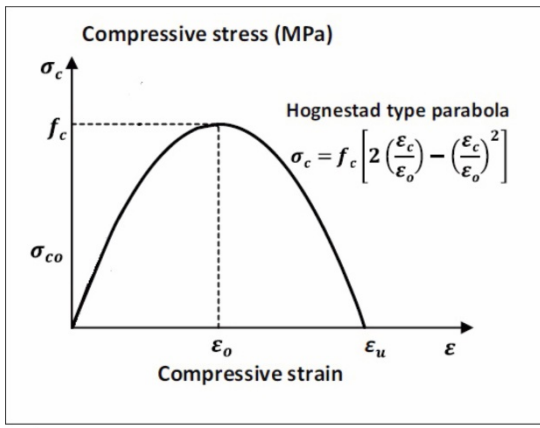
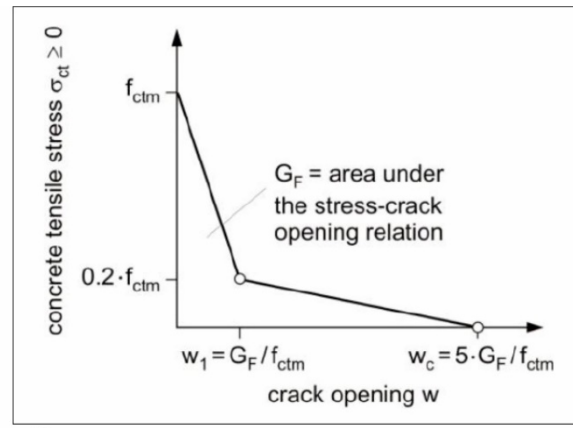


Fig. 17. Comparison between load-deflection curves obtained with Abaqus/Standard and Abaqus/Explicit for $T=0$ and $T/T_{cr}=0.8$



a)



b)

Fig. 18. a) Uniaxial compressive stress-strain relationship for concrete. b) Uniaxial tensile stress-crack width relationship for concrete

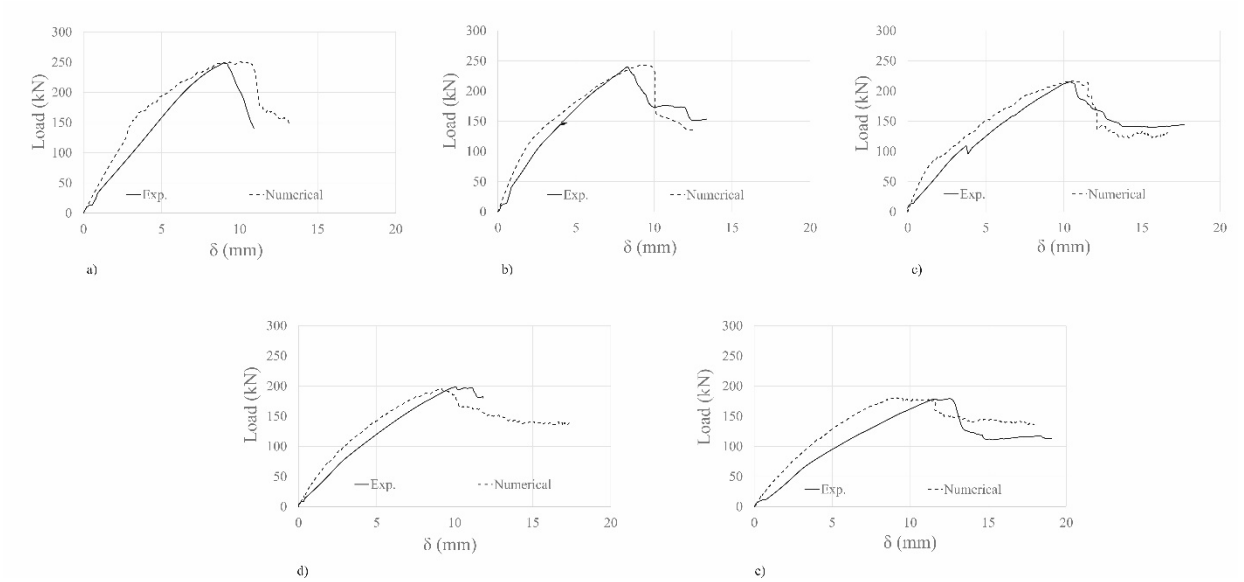


Fig. 19. Comparison between load-deflection curves obtained with the numerical model and in the laboratory tests for a) $T=0$; b) $T/T_{cr}=0.44$; c) $T/T_{cr}=0.69$; d) $T/T_{cr}=1.02$; e) $T/T_{cr}=1.26$.

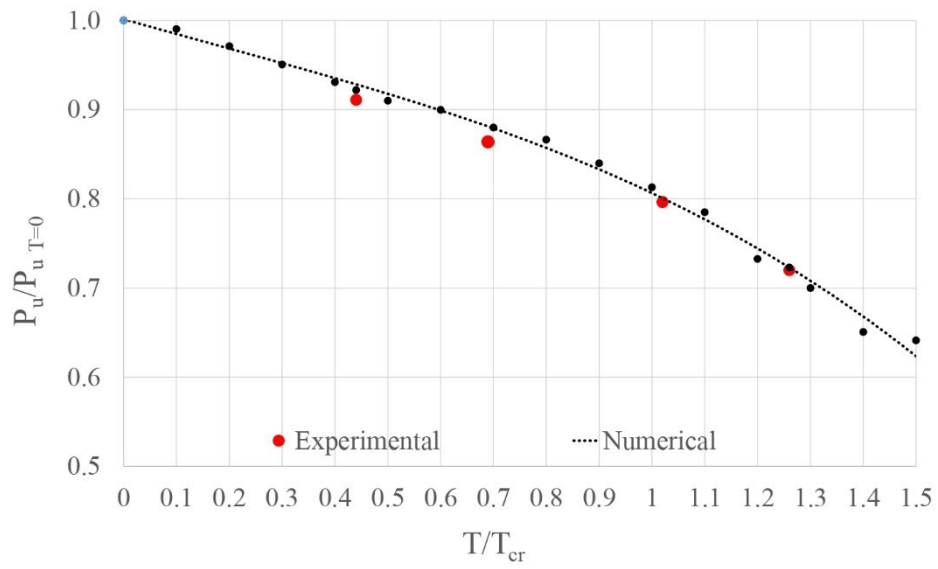


Fig. 20. Comparison of the relative decrement of the punching strength to the tensile force applied obtained numerically and in laboratory tests.

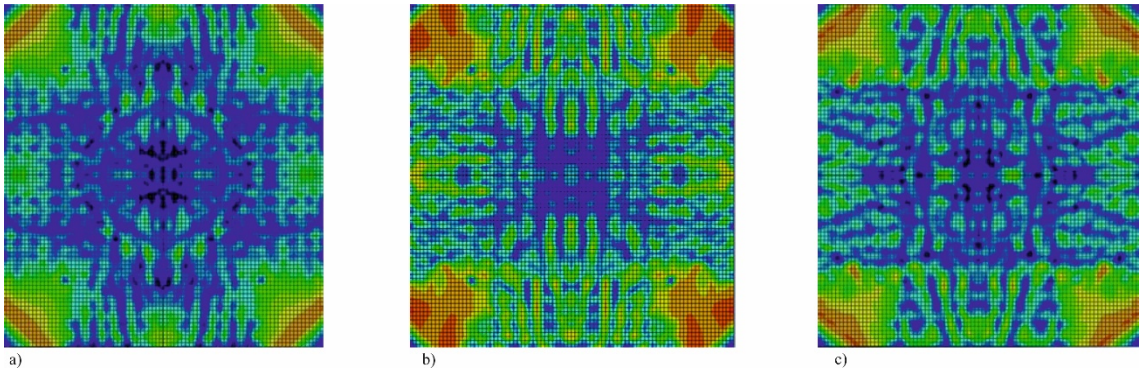


Fig. 21. Cracking pattern at failure for a) $T=0$; b) $T/T_{cr}=0.7$; c) $T/T_{cr}=1.26$; (Tensile force applied in vertical direction)